Molecular Biology of the Cell
Vol. 15, 838–850, February 2004

Reassessing the Role and Dynamics of Nonmuscle Myosin II during Furrow Formation in Early *Drosophila* Embryos[D][V]

Anne Royou,[*†] Christine Field,[‡] John C. Sisson,[†] William Sullivan,[†] and Roger Karess[*§]

*CNRS Centre de Génétique Moléculaire, 91198 Gif-sur-Yvette, France; [‡]Department of Cell Biology, Harvard Medical School, Boston, Massachusetts 02115; and [†]Department of Molecular, Cell and Developmental Biology, Sinsheimer Laboratories, University of California at Santa Cruz, Santa Cruz, California 95064

Submitted June 26, 2003; Revised October 9, 2003; Accepted October 10, 2003
Monitoring Editor: Mary Beckerle

The early *Drosophila* embryo undergoes two distinct membrane invagination events believed to be mechanistically related to cytokinesis: metaphase furrow formation and cellularization. Both involve actin cytoskeleton rearrangements, and both have myosin II at or near the forming furrow. Actin and myosin are thought to provide the force driving membrane invagination; however, membrane addition is also important. We have examined the role of myosin during these events in living embryos, with a fully functional myosin regulatory light-chain–GFP chimera. We find that furrow invagination during metaphase and cellularization occurs even when myosin activity has been experimentally perturbed. In contrast, the basal closure of the cellularization furrows and the first cytokinesis after cellularization are highly dependent on myosin. Strikingly, when ingression of the cellularization furrow is experimentally inhibited by colchicine treatment, basal closure still occurs at the appropriate time, suggesting that it is regulated independently of earlier cellularization events. We have also identified a previously unrecognized reservoir of particulate myosin that is recruited basally into the invaginating furrow in a microfilament-independent and microtubule-dependent manner. We suggest that cellularization can be divided into two distinct processes: furrow ingression, driven by microtubule mediated vesicle delivery, and basal closure, which is mediated by actin/myosin based constriction.

INTRODUCTION

Cytokinesis is the final step of cell division, required for the equal partitioning of the newly separated genetic material into two sister cells. Conventional animal cell cytokinesis is characterized by the assembly of an actin-myosin–based structure called the contractile ring, positioned midway between the two spindle poles, which drives the formation of a cleavage furrow. Despite its importance, many aspects of cytokinesis remain obscure. For example, although it is now well established that the cleavage plane can be specified by the central spindle or by astral microtubules (reviewed in Glotzer, 2001; Straight and Field, 2000), it is not known how microtubules trigger the assembly of the contractile ring or if they are required for regulating the contractile force.

During the early phase of *Drosophila* embryogenesis, the embryo undergoes 13 rounds of nuclear division in the absence of cytokinesis. However, two kinds of membrane invagination events believed to be mechanistically related to conventional cytokinesis take place: metaphase furrow formation and cellularization. Metaphase furrows, or pseudocleavage furrows, form transiently during the 10th to 13th mitotic cycles of the cortical syncytial divisions. At interphase, actin is concentrated in cortical caps above each nucleus, but with entry into mitosis, the actin cytoskeleton reorganizes from caps to rings at the base of shallow furrows surrounding each developing spindle (Zalokar and Erk, 1976; Foe and Alberts, 1983; Karr and Alberts, 1986; Foe *et al.*, 2000). These furrows form at prophase and reach a maximum depth at metaphase, thus creating a barrier separating each mitotic spindle and preventing them from colliding (Stafstrom and Staehelin, 1984; Sullivan *et al.*, 1990; Schejter and Wieschaus, 1993; Sullivan and Theurkauf, 1995). The furrows then regress during telophase. At least two myosins species are associated with furrows: classical nonmuscle myosin II (Kiehart, 1990; Young *et al.*, 1991; Field and Alberts, 1995; Foe *et al.*, 2000) and the short tail myosin VI, which has been shown to be required for furrow formation (Mermall and Miller, 1995).

The second event related to conventional cytokinesis is cellularization. This process, occurring just after completion of the 13th nuclear cycle of the syncytial blastoderm, is characterized by the invagination of the plasma membrane between each cortically positioned nucleus to a depth of ~30 μm and results in the simultaneous formation of the 6000 columnar epithelial cells of the cellular blastoderm. Immunofluorescence studies have found that both actin and my-

Article published online ahead of print. Mol. Biol. Cell 10.1091/mbc.E03–06–0440. Article and publication date are available at www.molbiolcell.org/cgi/doi/10.1091/mbc.E03–06–0440.

[D][V] Online version of this article contains supplemental material and videos. Online version is available at www.molbiolcell.org.

[§] Corresponding author. E-mail address: karess@cgm.cnrs-gif.fr.

Abbreviations used: GFP, green fluorescent protein; Drok, Drosophila rho kinase; MHC, myosin heavy chain; MLCK; RLC, regulatory myosin light chain; TLCM, time-lapse confocal microscopy.

© 2004 by The American Society for Cell Biology

osin II undergo dramatic rearrangements during this process (Warn *et al.*, 1980; Warn and Magrath, 1983; Young *et al.*, 1991). At the onset of cellularization, the actin cytoskeleton forms a hexagonal network around the nuclei. During furrow invagination, these proteins accumulate at the leading edge of the invaginating membrane. Once the furrows pass the level of the nuclei, they reorganize to form discrete rings that close off the cells basally. Drugs and mutations disrupting the integrity of the actin network all affect membrane invagination (Zalokar and Erk, 1976; Foe and Alberts, 1983; Kiehart, 1990; Schweisguth *et al.*, 1990; Simpson and Wieschaus, 1990; Schejter *et al.*, 1992; Foe *et al.*, 1993). Thus, contraction of this actin array has been postulated to provide a mechanistic force driving invagination (Warn and Magrath, 1983).

Metaphase furrow formation and cellularization share several properties with conventional cytokinesis: both kinds of invaginations involve actin cytoskeleton rearrangements, and this reorganization depends (directly or indirectly) on microtubules (MTs; Zalokar and Erk, 1976; Foe and Alberts, 1983; Edgar *et al.*, 1987; Warn *et al.*, 1987; Foe *et al.*, 2000). In addition, several other known cortical components of the classical cytokinesis contractile rings are found concentrated within the metaphase furrows and the furrow canals of cellularizing embryos (Zalokar and Erk, 1976; Foe and Alberts, 1983). These include myosin II (Kiehart, 1990; Young *et al.*, 1991; Field and Alberts, 1995; Foe *et al.*, 2000), anillin (Miller *et al.*, 1989; Field and Alberts, 1995), the formins (Afshar *et al.*, 2000), and the septins (Neufeld and Rubin, 1994; Fares *et al.*, 1995; Field *et al.*, 1996). However, the specific roles played by these other cortical components during these membrane invaginations are still unclear.

To date all published studies of *Drosophila* myosin II dynamics have been based on the examination of fixed and immunostained material. Although such studies have been extremely informative, it is likely that many aspects of myosin II dynamics have escaped attention because of the constraints of examining fixed material and extrapolating from population sampling. By taking advantage of the *spaghetti squash* (*sqh*) gene encoding the myosin II regulatory light chain (RLC), we constructed an RLC-GFP chimera to label myosin II in living *Drosophila* embryos. With this tool, we have obtained a refined description of the dynamics of furrow invaginations, in both normal and experimentally perturbed embryos. We find that both metaphase furrows and the membrane invaginations of cellularization can occur even in the presence of significant perturbation of myosin II behavior and activity. Finally, we identify a previously unrecognized reservoir of myosin II material that seems to be recruited basally into the invaginating furrow in a microtubule-dependent manner during the initial phase of cellularization.

MATERIALS AND METHODS

Fly Stocks

Flies were raised on standard corn meal *Drosophila* medium at 25°C. The isolation and cloning of sqh^{1} and sqh^{AX3} are described in Karess *et al.* (1991) and Jordan and Karess (1997)). The FLP-DFS system of Chou and Perrimon (1992) and Chou *et al.* (1993) was used to generate homozygous sqh^{1} germline clones as described by Wheatley *et al.* (1995). The stocks of *FRT101* and ovo^{D1} *FRT101/Y; hs-flp38* used to generate germline clones were obtain from Dr. N. Perrimon. Wild-type controls used the stock $y\ w^{67c}$, obtained from the Bloomington Stock Center. The stock sqh^{AX3}*; sqh-gfp42* described below was used for studying myosin behavior. The embryos produced by this strain are called in the text "RLC-GFP embryos." The stock GFP-Moesin is described in Edwards *et al.* (1997).

RLC-GFP Construct

We initially constructed both the N-terminal (*gfp-sqh*) and the C-terminal (*sqh-gfp*) versions of the chimera, both under the control of the natural *sqh* promoter. The *sqh* fragments were amplified by PCR using modified primers to introduce an Age I site and using as template DNA the Bluescript SK+ vector (Stratagene) containing a 0.75-kb *Eco*R1 fragment of genomic sqh^{+} (described in Karess *et al.*, 1991; Jordan and Karess, 1997). The fragments encoding the green fluorescent protein (GFP) mutant variant S65T (Clonetech), were generated with the Age I and *Xma*I ends and cloned into the Age I site of the *sqh* vector. These chimera *sqh-gfp* and *gfp-sqh* genes were cloned into the polylinker of the P transformation vector CasPer (Pirrotta, 1988), which carries in addition the selectable marker $mini\text{-}white^{+}$, and introduced into the germ line of $y\ w^{67}$ flies by standard methods (Karess *et al.*, 1991; Jordan and Karess, 1997). Only the sqh-gfp chimera fully complemented the null sqh^{AX3} in a single copy, (although the N-terminal chimera also produced viable adults), and this construct is used in the experiments described. See Supplemental Figure SF1 for the complete coding sequence of the *sqh-gfp* transgene.

Embryo Immunostaining

Immunofluorescence analysis was performed as described by Karr and Alberts (1986). yw^{67} embryos were dechorionated in 50% Clorox bleach solution and fixed in heptane solution presaturated with 37% formaldehyde in methanol during 45 min at RT. The postfix treatment was described by Rothwell and Sullivan (2000). The fixed embryos were pipetted onto a piece of Whatmann paper, allowing the heptane to evaporate, and then transferred to double-stick tape in the lid of a small Petri dish and covered with PBTA buffer (1× PBS, 1% BSA, 0.05% Triton X-100, 0.02% NaN_3). The vitelline membranes were removed by hand with a needle under a microscope. The embryos were incubated with the rabbit anti-Anillin antibodies used at 1/1000 (Field and Alberts, 1995), or rabbit anti-MHC at 1/1000 (Wheatley *et al.*, 1995). Bound antibodies were detected using a goat anti-rabbit IgG secondary antibody conjugated to Cy5 (Molecular Probes, Eugene, OR). F-actin was labeled using phalloidin conjugated to Alexa 488 (Molecular Probes). To visualize DNA, embryos were treated with 10 μg/ml RNase for 2 h at 37°C, followed by extensive rinsing in 1× PBS and mounted in a 90% glycerol, PBS solution containing 1 μg/ml *N-N*-1–4-phenylenediamine and 1 mg/ml propidium iodide.

Microinjection and Imaging of Live Embryos

Embryos were prepared for microinjection and time-lapse scanning confocal microscopy (TLCM) according to Francis-Lang *et al.* (1999), by being removed from the chorion, dehydrated briefly, and covered with halocarbon oil. The following reagents were injected at the 50% egg length at approximately 1% of the egg volume: rhodamine-conjugated tubulin (10 mg/ml, Molecular Probes), cytochalasin B and latrunculin (0.2 mM in 40% DMSO; Sigma-Aldrich, St. Louis, MO), colchicine (1 mM in H_2O; Sigma-Aldrich), cycloheximide (0.2 mM in DMSO), Y-27632 (50 mM in H_2O; Calbiochem, La Jolla, CA), and anti-MHC (polyclonal affinity purified). Embryo injection was performed as described in Foe and Alberts (1983). Intracellular concentrations of the injected reagents were diluted ~100 fold. Scanning confocal movies were started within 20 s after injection. The doses of cytochalasin and colchicine used were sufficient to eliminate F-actin and tubulin in syncytial embryos (actin caps and metaphase furrows, and spindles, respectively).

Confocal Microscopy and Time-Lapse Recording

Microscopy was performed using a Leitz DMIRB inverted microscope (Wetzlar, Germany) equipped with a Leica TCS NT laser confocal imaging system (Wetzlar, Germany). Images of the time series result from scans (with 3 accumulations) every 15, 30, or 60 s. Leica TCS NT and Metaview imaging system (Universal Imaging, Downingtown, PA) were used for quantification. Curves were made using Kaleidagraph (Synergy Software, Reading, PA). Rates of furrow invagination were calculated by linear extrapolation (n = 3).

RESULTS

Construction and Analysis of the Fusion Protein RLC-GFP

We constructed a sqh-GFP chimerical transgenic, where the GFP sequence was fused to the C-terminus of the RLC, expressed under the control of the natural *sqh* promoter in a P element transformation vector and used to establish transgenic *Drosophila* lines (Supplemental Figure SF1). Three independent transformed lines were obtained and all fully rescued the null sqh^{AX3} allele. Although the homozygous sqh^{AX3} died at the first instar larval stage, all the transgenic lines rescued sqh^{AX3} to fertile adults when present in two

copies, and one line (line C-42) completely rescued even when present in a single copy. The individuals showed no polyploidy in the dividing tissues examined and no obvious phenotype except for a weak curvature of the wings in some individuals heterozygous for the transgene. Therefore, the 27-kDa GFP moiety placed at the C terminus of the 20-kDa RLC apparently does not interfere with normal RLC function.

The fluorescence intensity of line C-42 in a wild-type (sqh^+) background was substantially weaker than in a sqh^{AX3} background, suggesting that the binding of endogenous RLC to its IQ domain on the MHC competes with RLC-GFP. Consequently, the experiments described herein all used a stock expressing RLC-GFP in the null sqh^{AX3} background. This stock is referred to as "RLC-GFP" flies.

Myosin II Dynamics during Cellularization

Using the RLC-GFP line, we examined myosin II behavior during cellularization by time-lapse confocal microscopy (TLCM; Figure 1A and Movie 1), measuring both the rate of the furrowing and the fluorescence intensity at the front (Figure 1B; Table 1). As has been reported before (Schejter and Wieschaus, 1993), the rate is biphasic, comprised of a slow phase of roughly 0.2 μm/min (see Table 1), and a fast phase of 1 μm/min, beginning ~30 min into cellularization. Thereafter the rate remained constant until the end of cellularization at ~60 min. During the slow phase, myosin II fluorescence at the front increased at a constant rate (Figure 1B, intensity curve), reflecting apparently the progressive recruitment of myosin II to the leading edge as it formed a hexagonal network around the nuclei (Figure 1, A and B). As reported by others, little myosin II was found along the lateral plasma membranes or along the surface of the embryo (Warn *et al.*, 1980; Young *et al.*, 1991). The fluorescence intensity reached a plateau at 30 min, just when the furrow was accelerating. At this stage myosin II reorganized into discrete rings that progressively contracted during the fast phase (Figure 1B, bottom panels). At roughly 40 min, when the furrows had deepened to ~17 μm, the fluorescence began to rapidly decline. However, in fixed embryos stained with anti-MHC antibody, the fluorescence at the front stayed constant until the very end of cellularization (unpublished data), suggesting that decrease in fluorescent signal is caused by quenching once the front has reached the vitellus.

Myosin II Is Recruited to the Furrow Front from a Cytoplasmic Reservoir

During the slow phase of cellularization numerous RLC-GFP particles could be seen just beneath the front (Figure 2 and Movie 2). These particles, ~1–2 μm in diameter, were particularly abundant at the onset of furrowing and their number decreased progressively over the next 20 min. The particles typically oscillated stochastically and then moved apically toward the advancing furrow, where they visibly fused. The apically directed motion had an approximate velocity of 0.04 μm/s. By the end of the slow phase, no more particles could be seen incorporating into the myosin-enriched front (unpublished data but see Figure 3, control). The videos (e.g., Movie 2) strongly suggest that the particles are a major source of the increased GFP signal at the front. This conclusion is supported by the drug and antibody injection studies described below.

To further characterize these particles, RLC-GFP embryos were fixed and immunostained with a variety of probes (unpublished data). All the GFP particles labeled with anti-MHC, indicating that they probably contain intact myosin II. Two thirds of the particles colocalized with actin particles (first seen by Warn and Robert-Nicoud, 1990) found just beneath the furrow front. By contrast, the myosin particles did not colocalize with βCOP P120, Lva, or the vesicle-associated Dah, all of which are markers for Golgi-derived vesicles (Ripoche *et al.*, 1994; Rothwell *et al.*, 1999; Sisson *et al.*, 2000; Zhang *et al.*, 2000), nor did they label with antiphospho-tyrosine (a membrane marker). The myosin puncta therefore do not appear to be associated with membrane vesicles. Moreover, their behavior is distinct from the membrane vesicles described by Lecuit and Wieschaus (2000), which fuse laterally with the furrows, and not at the leading edge.

All three RLC-GFP transgenic lines have the large cytoplasmic myosin II particles when expressed in a sqh^{AX3} mutant background, where no endogenous RLC is present, and the GFP-myosin puncta are also visible in wild-type embryos bearing four copies of the RLC-GFP transgene. However, we have been unable to find particles of a similar size in fixed preparations of wild-type embryos not expressing RLC-GFP. Fixed wild-type embryos do show numerous very small myosin II–containing particles just beneath the cellularization front (unpublished data). Thus the possibility exists that the large myosin II particles are artifacts of the GFP-RLC chimera. We point out, however, that the RLC-GFP particles themselves are very sensitive to fixation conditions, requiring a special protocol to be preserved (see MATERIALS AND METHODS). We discuss further the nature of these particles in the DISCUSSION.

The Apical Movement of Myosin II Particles Requires Microtubules

F-actin depolymerization with cytochalasin B had no obvious effect on the myosin II particles' apical movement (Figure 3, last row; see also Movie 4). However, the particles generally did not fuse with the furrow, but continued to move apically until they could be found above the nuclei (arrowheads). This failure to fuse is mostly likely a simple consequence of the disintegration of the myosin II network at the front. Colchicine treatment by contrast arrested nearly all the movement of the myosin II particles (Figure 3, second row, arrows; see also Movie 3), suggesting that the particles are moving along MTs. Because at this time in the early embryo MTs form an inverted basket around each interphase nucleus, with their minus ends oriented apically (Foe and Alberts, 1983), one possibility is that the myosin II puncta move apically via a minus-end–directed MT motor protein (see DISCUSSION).

Effects of Perturbing Cytoskeleton on Cellularization Furrow Invagination and Myosin II Behavior

It is well established from studies of fixed embryos that colchicine or cytochalasin treatment blocks cellularization (Zalokar and Erk, 1976; Foe and Alberts, 1983; Edgar *et al.*, 1987; Warn *et al.*, 1987; Sisson *et al.*, 2000). We took advantage of the RLC-GFP marker to specifically follow the in vivo dynamics of furrow progression and myosin II network reorganization in response to various treatments (Table 2).

Microtubules. The depolymerization of MTs (Figure 3 and Movie 3) by colchicine injection (1 mM) at the onset of cellularization almost completely blocked furrow formation (unpublished data). Injection 20 min after the onset of cellularization immediately slowed furrow ingression almost to a stop (Figure 3, second row; see also Foe and Alberts, 1983). Furrows eventually just bypassed the nuclei, but did not progress further. Surprisingly, however, this late treatment with colchicine did not obviously perturb the reorga-

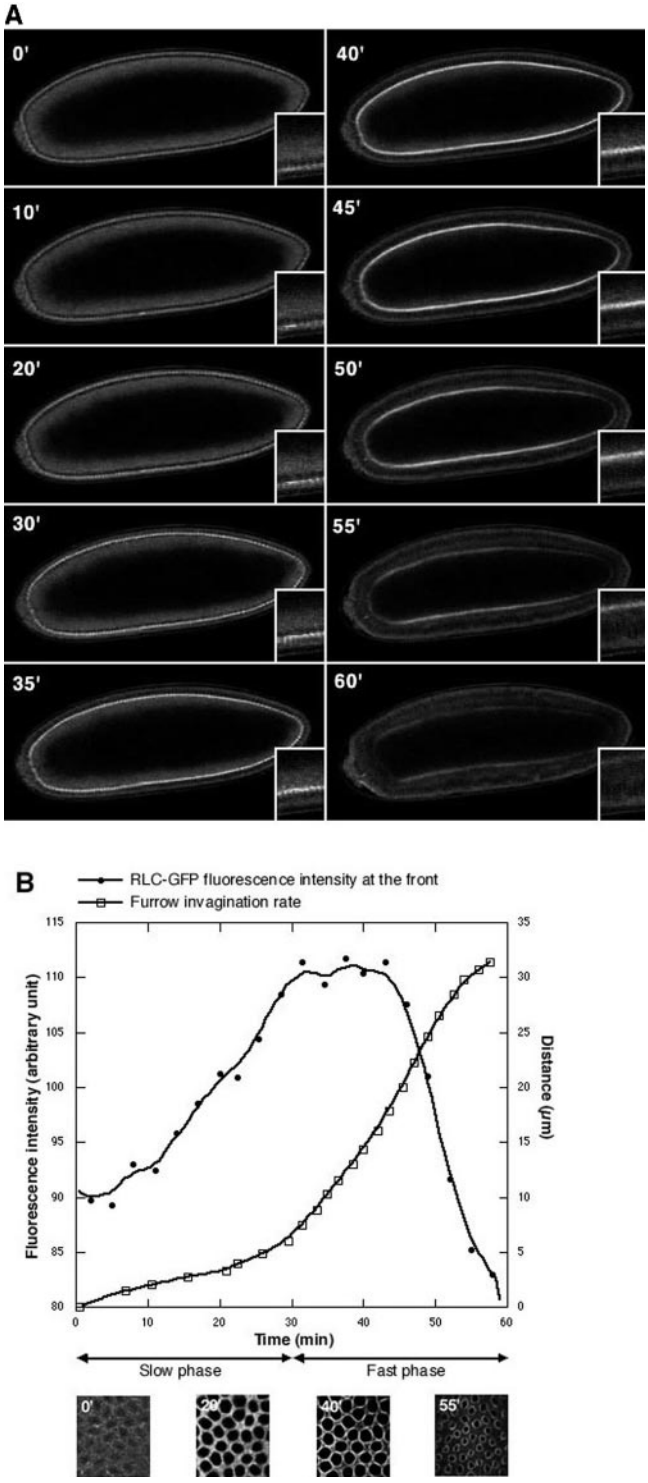

Figure 1. Myosin II behavior during cellularization. (A) Cross section of an RLC-GFP embryo examined by TLCM from the onset (t = 0 min) to the end (t = 60 min) of cellularization. Insets: part of the cortex at high magnification. Note the accumulation of fluorescence at the furrow front. (B) Typical curves of the RLC-GFP fluorescence intensity at the front and the furrow invagination rate (dorsal) are shown. The fluorescence intensity at the front progressively increases and reaches a plateau at 30 min, the period corresponding to the slow phase of cellularization. Around 30 min, the furrow enters the fast phase, and invagination accelerates. After 50 min, the fluorescence intensity rapidly decreases as the furrow front reaches the vitellus at a depth of roughly 20 μm. The furrow invagination stops at 60 min, having reached its maximum depth of >30 μm. The bottom panels are apical views of the furrow front at different periods of a cellularization. During the slow phase (first and second panels), the fluorescence accumulates around the nuclei to form a hexagonal network. During the fast phase, it reorganizes into distinct rings (third panel) that progressively decrease in diameter (last panel). Time in minutes. See also Movie 1.

Table 1. Furrow invagination rates during slow and fast phases

Furrow invagination rates (μm/min)	
Slow phase	Fast phase
0.179 ± 0.015 (n = 3)	1.007 ± 0.020 (n = 3)

nization of myosin II from hexagonal arrays into distinct rings that normally occurs during the fast phase, and more significantly, did not block their subsequent closure at the base of the cells. Indeed, these myosin rings contracted apparently normally at the expected time, beginning ~50 min after furrow onset. This result suggests that the transition from slow phase invagination to basal closure is triggered not by the furrow reaching a given depth, but rather by a clock marking time with respect to the onset of cellularization (see DISCUSSION).

Actin. Depolymerization of actin filaments by cytochalasin (0.2 mM) at different stages of cellularization had different effects on furrow structure and invagination (Figure 3 and Movie 4). Injection of cytochalasin just at the onset of cellularization completely blocked furrow ingression (unpublished data) as has been described by others (Zalokar and Erk, 1976). When the drug was injected 20 min after the onset of cellularization (Figure 3, fourth row), when actin and myosin had already been recruited to the front, the treatment did not block furrow ingression. Instead, furrowing continued, (albeit somewhat more slowly) despite the fact that the drug severely reduced the myosin in the furrow front. Large gaps appeared in the myosin network, and by the end of the invagination period little myosin remained in the furrows. In contrast to the continued furrowing, there was no evidence of basal closure in these embryos. Latrunculin treatment had a similar effect (unpublished data).

Myosin. To assay the importance of myosin in cellularization, we took both genetic and pharmacological approaches to perturb myosin function. The strong hypomorphic *sqh*^{1} allele reduces myosin RLC levels by at least 90% and leads to defects in cytokinesis, oogenesis, axial expansion, and other aspects of development (Karess *et al.*, 1991; Wheatley *et al.*, 1995; Edwards and Kiehart, 1996; Jordan and Karess, 1997). Moreover, the reduced amount of the RLC in *sqh*^{1} mutant tissues causes severe disruption of the myosin network, because the MHC forms nonfunctional aggregates (Wheatley *et al.*, 1995; Edwards and Kiehart, 1996). Figure 4 compares the myosin distribution in syncytial stage wild-type embryos and embryos derived from homozygous *sqh*^{1} germline clones (referred to as sqh^{1} embryos). Although in the wild-type a robust myosin II network covers the embryonic cortex, in sqh^{1} embryos, myosin II is present only in short discontinuous patches and in some regions is almost entirely absent.

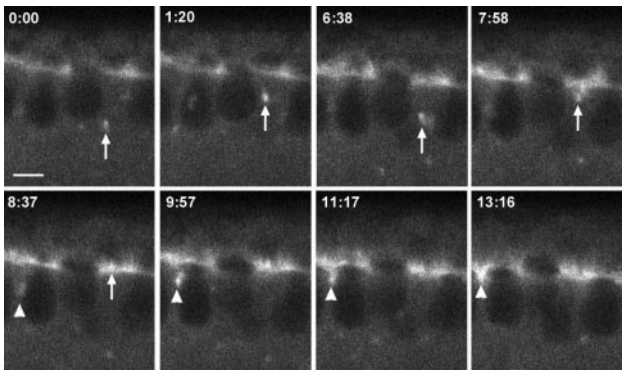

Figure 2. Particles containing cytoplasmic myosin II move apically to fuse with the furrow front. High magnification of the cortex of an RLC-GFP embryo visualized by TLCM during the slow phase of cellularization. Black holes correspond to the nuclei, and the fluorescent line above the nuclei corresponds to the furrow front. Numerous particles of myosin (arrows and arrowheads) are found just beneath the furrow front. In this series, the movements of two particles are followed. The first particle (arrow) shows saltatory movements toward and away from the furrow before finally getting incorporated into the front. The second particle (arrowhead) moves directly apically and fuses with the front. During this period the overall fluorescence at the front progressively increases (compare the first and the last panel; see also Figure 1B). Scale bar, 4 μm. Time, min:sec. The saltatory movement and fusion of the particles can be better appreciated in Movie 2.

We compared cellularization in living wild-type and sqh^1 embryos by time-lapse DIC microscopy (Figure 5A). As a result of the axial expansion failure typical of sqh^1 embryos (Wheatley *et al.*, 1995), the anterior half of the embryo begins to cellularize before the posterior (Figure 5). This limit is clearly seen (arrowhead of the first sqh^1 embryo frame). The furrow front is visible as a thin dark line and is marked by arrows in each embryo. Once initiated, the furrows of the sqh^1 embryo proceeded at a roughly normal speed and depth. After 45 min, as the furrow front at the anterior half was nearly at its maximum depth, it was only beginning to invaginate near the posterior pole (arrowhead). At the end of cellularization, the leading edge of the furrow reached the vitellus (dark area) and is no longer visible.

Anti-MHC staining of fixed wild-type and sqh^1 embryos at the end of cellularization (Figure 5B) revealed that in both embryos myosin II was found at the furrow base. However in wild-type, the myosin formed small contracted rings, whereas in sqh^1 embryos, the myosin was present in irregular aggregates (Figure 5B, surface view).

Another way to specifically disrupt myosin II activity is by inhibition of *Drosophila* rho kinase (Drok) with the drug Y-27632, a specific Rho kinase inhibitor (reviewed in Narumiya *et al.*, 2000). Rho kinase appears to be the principle enzyme regulating RLC phosphorylation in *Drosophila*, acting both to inhibit the myosin phosphatase and to directly phosphorylate the activating serine and threonine of the RLC (Amano *et al.*, 1996; Kimura *et al.*, 1996; Fukata *et al.*, 2001; Winter *et al.*, 2001). Without these phosphorylations, myosin II is essentially inactive. Treatment of early syncytial stage *Drosophila* embryos with Y-27632 has been shown to

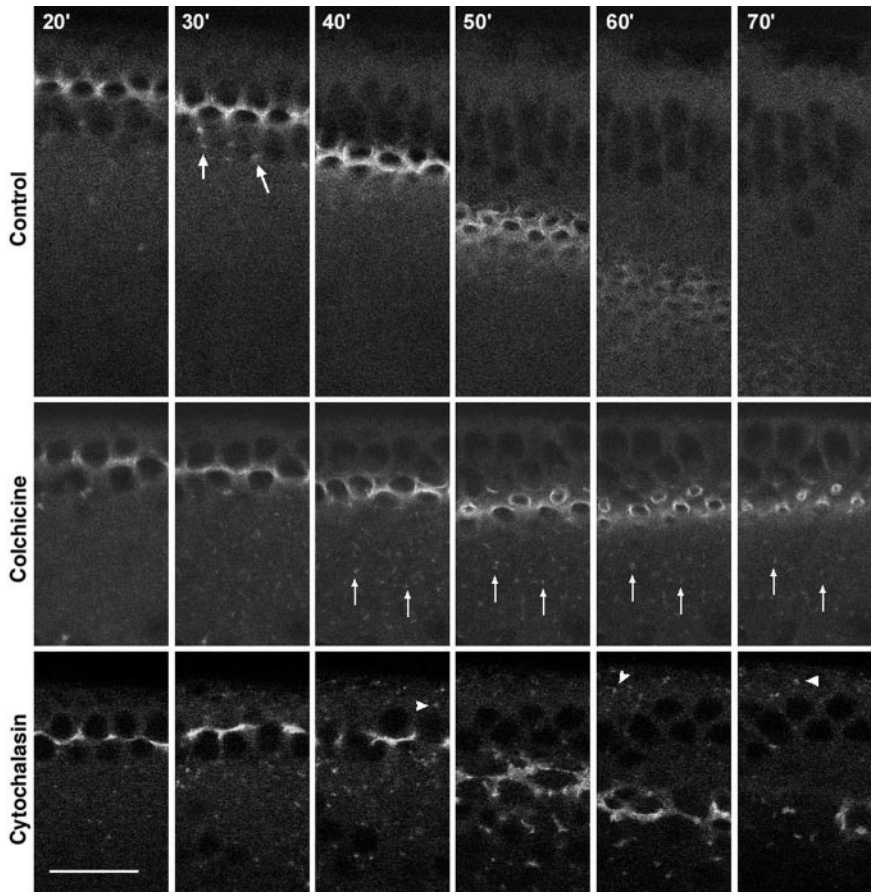

Figure 3. The effects of colchicine and cytochalasin on cellularization. Myosin reorganization into rings and subsequent ring contraction during the fast phase of cellularization requires F-actin but does not require microtubules and occurs even without complete furrow invagination. All panels are pseudosagittal views of RLC-GFP embryos monitored by TLCM. The drugs were injected 20 min after the onset of cellularization. The first panels of each injected embryo are scanned a few seconds after injection of DMSO (control), colchicine (1 mM), or cytochalasin (0.2 mM). Control embryos (top row) undergo normal furrowing. Some myosin puncta can be seen below the front at 20 and 30 min into cellularization and have been totally incorporated into the front by 40 min. See also Movie 2. Colchicine injection (second row) at 20 min almost entirely inhibits furrow invagination and myosin particle movements (arrows). However, the myosin ring contraction characteristic of the second half of the fast phase occurs at the expected time (compare with control embryos) during the last 15 min. See also Movie 3. Cytochalasin injection (bottom row) at 20 min only mildly affects furrow invagination, which progresses nearly as deeply as in the control, yet the myosin network is profoundly disrupted. Cytochalasin treatment has no effect on myosin particle movement, but as the myosin-rich front is disrupted, some puncta pass beyond the front and are found apically (arrowhead). Scale bar, 20 μm. Time (min) is relative to the onset of cellularization. See also Movie 4.

Table 2. Effect of different treatments on furrow invagination and myosin behavior

Drug	Time of injection[a]	Furrow initiation	Furrow ingression	Myosin network at front	Basal ring contraction	Myosin particle movement
Colchicine (1 mM)						
	Early	No				
	Late		Blocked	Intact	Normal	Arrested
Y27632 (50 mM)						
	Early	Yes		Absent		
	Late		Continues	Absent	Defective	No particles
Cytochalasin B (0.2 mM)						
	Early	No	Blocked			
	Late		Continues[b]	Disrupted	Defective	Normal[c]

[a] Early injection is just before the onset of cellularization. Late injection is 20 min after onset.

[b] Ingression continues, but is slower and does not reach normal depth.

[c] Particles still move apically, but many no longer fuse with the front. See text for details.

block nearly all myosin II recruitment to the embryonic cortex and indeed produces a phenocopy of the sqh mutant germline clones (Royou *et al.*, 2002).

We injected Y-27632 (50 μM) into interphase cycle 14 embryos just before the onset of cellularization. This treatment substantially inhibits the recruitment of myosin II to the invaginating furrows (Figure 6). Nevertheless, the furrows form, and continue to deepen, reaching ~20 μm by 40 min. After 40 min, the very faint myosin signal at the furrow front is no longer visible. Thus, disruption of myosin II function by genetic or by pharmacological means fails to block the first phase of cellularization, indicating that relatively little or possibly no myosin II activity is required for this process.

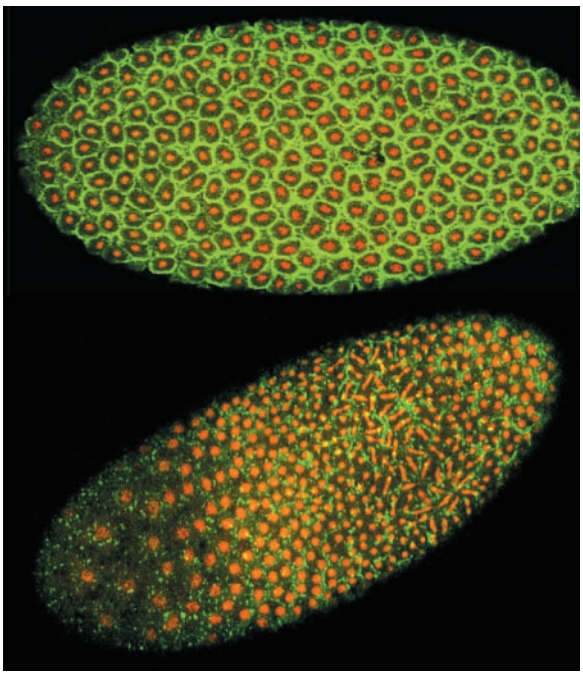

Figure 4. Myosin II distribution in wild-type and sqh[1] embryos. WT (top) and sqh[1] (bottom) syncytial blastoderm stage embryos, fixed and stained with anti-MHC (green). Nuclei (red) are labeled with propidium iodide. Wild-type embryos have a uniform uninterrupted network of myosin surrounding each nucleus. In sqh[1] embryos, the myosin network is severely disrupted and in some cases absent altogether. Much of the MHC is found in large aggregates. The dearth of nuclei at the posterior pole (left) reflects a defect in nuclear axial expansion (see Royou *et al.*, 2002).

Effects on Metaphase Furrow Invagination

Metaphase furrows are structures of critical importance to maintain the integrity of the syncytial mitotic spindles (Stafstrom and Staehelin, 1984; Sullivan *et al.*, 1990; Schejter and Wieschaus, 1993; Sullivan and Theurkauf, 1995). Even slight perturbations in metaphase furrow formation lead to collisions between neighboring spindles and consequent mitotic abnormalities. During the syncytial blastoderm stage of embryogenesis, myosin II undergoes cycles of cortical recruitment and dispersion in concert with the mitotic cycle (Foe *et al.*, 2000; Royou *et al.*, 2002). It is present at interphase and in fact is concentrated at the leading edge of the metaphase furrows as they form during prophase. However, myosin II disperses from the cortex during metaphase, just when furrows reach their maximum depth, suggesting that it might not be participating directly in the formation and maintenance of the metaphase furrows. This behavior distinguishes it from myosin VI, which associates with furrows in prophase and persists throughout metaphase (Mermall and Miller, 1995).

To assess the role of myosin II in metaphase furrow formation, we examined furrow assembly, cortical divisions, and actin organization in live embryos after anti-MHC antibody injection (Figure 7, A and B). Anti-MHC injection disrupted the myosin network at the site of injection, generating myosin aggregates at the cortex and in the cytoplasm (Figure 7A). These aggregates persisted during mitosis, when cortical myosin II in wild-type and control embryos normally disperses (Foe *et al.*, 2000; Royou *et al.*, 2002). Anti-MHC antibodies were then injected into embryos doubly labeled by expression of the fusion protein Moe-GFP, a good marker of cortical actin cytoskeleton (Edwards *et al.*, 1997), and by injection with rhodamine-tubulin (red). At entry into prophase, actin reorganized normally from cap to furrow, even at the site of anti-MHC injection (Figure 7B). Moreover, no defects in spindle formation or mitotic divisions were detected. Each spindle was correctly formed and encircled by the metaphase furrow. Because this is such a sensitive "assay" for the integrity of the metaphase furrows, we conclude that the disruption of the myosin II network by anti-MHC injection did not affect metaphase furrow formation, actin organization, or nuclear divisions.

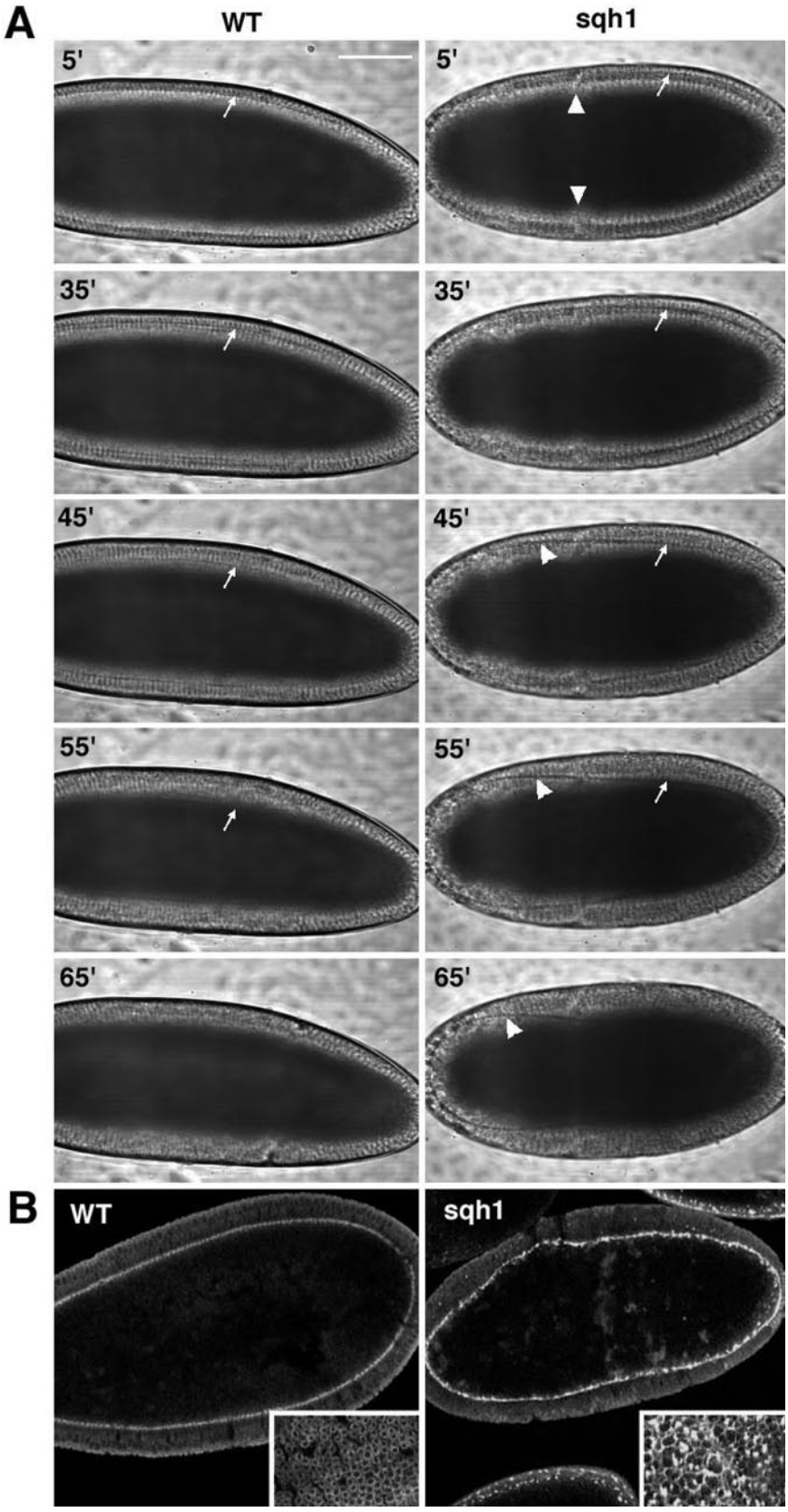

Figure 5. Cellularization progresses nearly normally in the sqh[1] embryo anterior half. (A) Time-lapse observation in DIC of wild-type and sqh1 mutant embryos during cellularization. Anterior of the embryos is to the right. The dark area of the interior of each embryo is the yolky cytoplasm. The transparent layer contains the cortical nuclei and the yolk-free cytoplasm. The cellularization front is visible in both wild-type and sqh[1] embryo mutant as a thin dark line and is marked by arrows. (5′ to 35′) slow phase, (45′ to 55′) fast phase, (65′) end of cellularization-onset of gastrulation with cephalic furrow formation (arrowhead) in wild-type embryo. (Scale bar, 80 μm). (B) Sagittal views of wild-type and sqh[1] embryos fixed and stained with anti-MHC antibody (green) and propidium iodide (red). Insets show an en face view at the plane of the furrow front. Myosin II is still present at the furrow front of sqh[1] embryos, but severely disorganized.

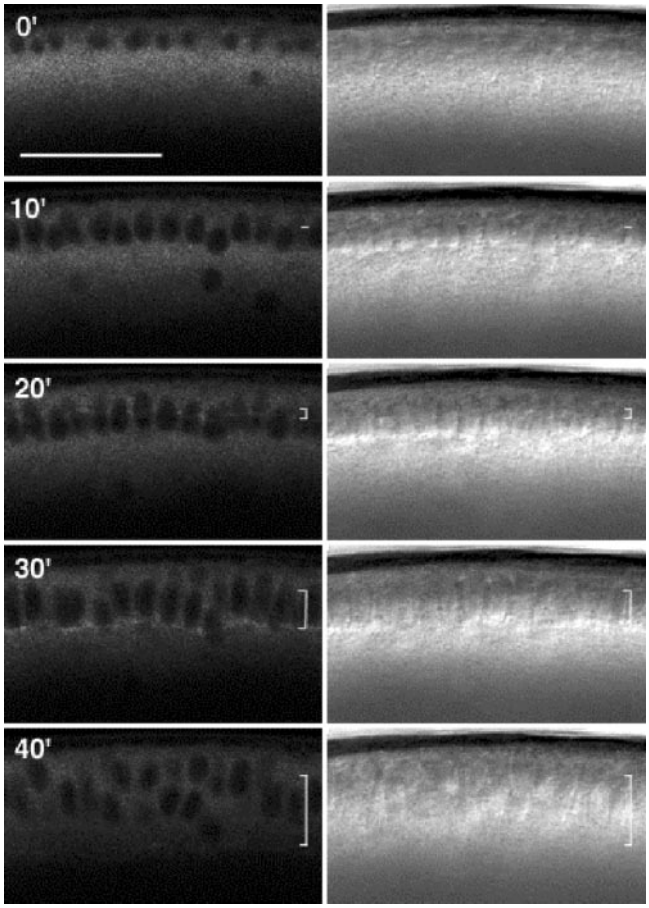

Figure 6. Cellularization occurs after Y-27632 injection. Time-lapse observation of RLC-GFP (left) and DIC (right) after Y-27632 injection at the onset of cellularization. Inhibiting Rho kinase with the drug Y-27632 substantially reduces myosin II recruitment to the cortex (see also Royou *et al.*, 2002), but furrows form and invaginate to a depth of 20 μm, 40 min after the onset of cellularization (see bracket). The rate of invagination is equivalent to normal embryos. The furrow is no longer visible after 40 min.

We also examined metaphase furrow formation in fixed sqh^1 embryos stained for actin, Anillin, and DNA (Figure 7C). Because the syncytial divisions of sqh^1 embryos are asynchronous due to the defect in nuclear axial expansion (unpublished observations), several waves of divisions propagate from the posterior toward the anterior pole. One such wave is shown in Figure 7C. At metaphase, actin colocalized normally with Anillin within the metaphase furrows, which have correctly formed around each spindle (see Figure 7C, sagittal view). At anaphase and telophase, the actin reconcentrated at each pole of the mitotic figures close to the new centrosome pair, and then reformed the cap above each nucleus. Anillin remained localized around the mitotic figures and then associated with each new nucleus, being excluded from the actin cap. Nor was there any evidence of spindle collision. Thus, in all respects, the behavior of actin and Anillin appeared normal in the cortical divisions of sqh^1 embryos. Inhibition of cortical myosin II recruitment by Y-27632 treatment similarly had no effect on furrow formation (unpublished data). We conclude from these studies that myosin II plays no critical role in the formation or maintenance of metaphase furrows.

Imaging Cytokinesis with RLC-GFP

We examined the RLC-GFP distribution of live mitotic cells during the first true cytokinesis events in a mitotic domain of the head region after cellularization (Figure 8A; see also Movie 5). During interphase, a diffuse homogenous GFP signal was detected in the cytoplasm, and outlining each cell, but excluded from the nucleus (cell 4 in Figure 8A). Just before nuclear envelope breakdown, myosin II accumulated rapidly at the cortex to form a fluorescently uniform layer just beneath the plasma membrane, as the cell rounded up (cell 3). During prometaphase and metaphase, some myosin was consistently detected on the spindle. Also apparent in the video images was a constant oscillation of the spindle, which only ended at anaphase onset (compare spindle position of cell 3 between 0:00 and 1:20; stars). At the start of anaphase, cortical myosin II began increasing at the equator of the cell and decreased first at the poles and then over the rest of the cortex, in a manner strongly suggesting cortical flow (arrowheads, cells 1 and 3). Once the contractile ring assembled, it contracted and pinched off rapidly to form two daughter cells (arrow cell 2). After completion of cytokinesis, some myosin lingered at the site of cleavage. By the next interphase, myosin II had largely disappeared from the cortex of both daughter cells and diffused back into the cytoplasm.

The behavior of myosin II was significantly altered when RLC-GFP embryos were injected with cytochalasin at the end of cellularization (Figure 8B). When the cells entered mitosis, myosin still accumulated at the cortex but in irregular patches and the cells did not completely round up. At anaphase, myosin did not accumulate at the equator and no contractile ring formed, and the cell elongated without dividing. Cytochalasin did not prevent formation of the central spindle in such cells, but it disappeared rapidly, suggesting that its stability was compromised by the absence of the contractile ring, as has been observed in *Drosophila* spermatocytes cytokinesis (Giansanti *et al.*, 1998). Finally, we examined cytokinesis in sqh^1 embryos fixed and stained for actin and DNA (Figure 8C). A large proportion of cells in these embryos failed to divide. The cells were generally smaller and no cleavage furrow formed at the equator (Figure 8C, second line). In some cases, an incomplete furrow could be found just below the apical surface of the cell (Figure 8C, third line, arrows). This furrow did not proceed all around the equator of the cell and penetrated only ~2 μm into the cell. Although this cytokinesis defect is most likely due to the lack of functional myosin in the contractile ring (Karess *et al.*, 1991), it is also possibly related to the failure of the cell to have competed cellularization.

DISCUSSION

A Minor Role for Myosin II in Furrow Invagination

We have monitored myosin II behavior during metaphase furrow formation accompanying the mitoses of syncytial blastoderm and during cellularization of syncytial embryos, in both wild-type and experimentally perturbed conditions. In doing so, we have been able to better define its dynamics and its role in this process. Our principle findings regarding myosin II are as follows: 1) furrow ingression during syncytial mitoses and during cellularization can occur even when myosin II activity is severely impaired; 2) myosin II plays an essential role in the last part of cellularization, basal closure; and 3) myosin II is, in part, recruited to the invaginating front of the cellularization furrow from a cytoplasmic pool.

The discovery of myosin II concentrations at the furrow front during cellularization naturally led to the long-stand-

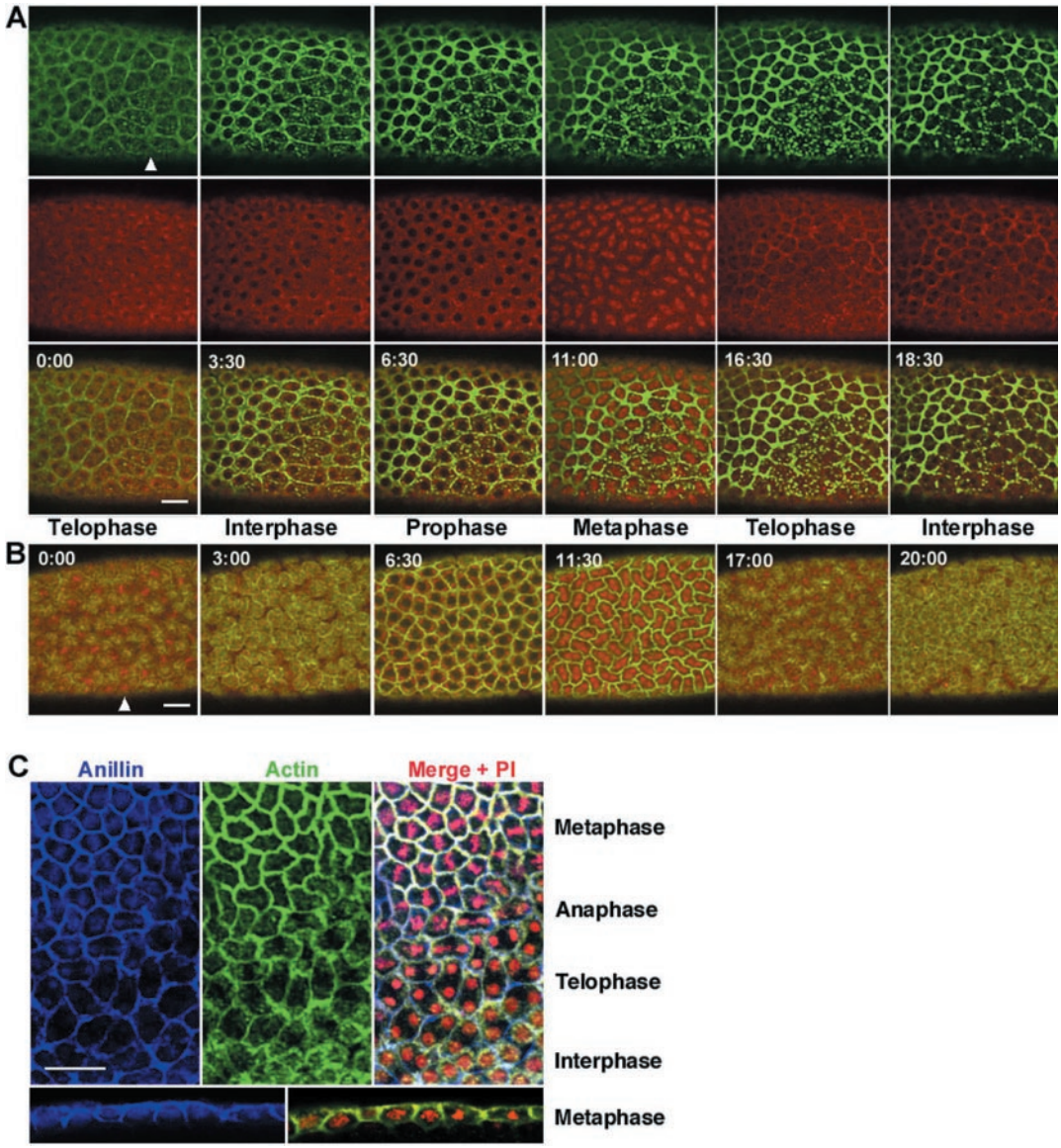

Figure 7. Myosin II is not required for metaphase furrow invagination. The panels in A and B are from scanning confocal movies of an RLC-GFP (green) embryo (A) and Moesin-GFP (green) embryo (B), both injected with rhodamine-tubulin (red) and anti-MHC antibody. (A) Anti-MHC antibody disrupts the myosin network at the site of injection (arrow) forming large aggregates, but has no effect on cortical divisions, indicating that the furrows still form to surround each spindle. (B) Anti-MHC antibody injection of embryos expressing GFP-Moesin (which marks the distribution of F-Actin (Edwards *et al.*, 1997) does not affect the reorganization of actin from interphase caps to metaphase furrows. (C) Metaphase furrows form normally in sqh^1 embryos. Fixed embryos were stained with antianillin (blue), phalloidin (green), and propidium iodide. The top panels are surface views and bottom panels are sagittal views of the same embryo. In sqh^1 embryos the cortical divisions are asynchronous, which leads to multiple waves of divisions. One such wave is seen in this surface view, from metaphase (top) to interphase (bottom). At metaphase, both anillin and actin concentrate in the metaphase furrow, and as the wave exits mitosis, actin reorganizes into interphase caps and anillin reorganizes around them. The sagittal views show the furrow fully invaginated around each metaphase spindle. (Scale bars, 20 μm).

ing assumption that it was involved in generating traction forces pulling down the membrane (Warn *et al.*, 1980; Kiehart *et al.*, 1990; Young *et al.*, 1991). We have shown here however by two different approaches, analysis of eggs produced from sqh^1 germline clones and inhibition of Rho kinase, that the membrane invaginations can occur quite well with substantially reduced levels of myosin II. These treatments did not block the initiation or the progression of the slow phase of cellularization, and during the fast phase the furrow continued ingressing, reaching approximately a normal depth. Although neither approach entirely eliminates myosin II activity, both the drug and the *sqh*^{1} mutation severely perturb other known myosin II–dependent processes such as cytokinesis and nuclear axial expansion (Karess *et al.*, 1991; Royou *et al.*, 2002). Taken together with our observation that even cytochalasin treatment does not fully arrest furrow ingression of cellularizing embryos, these results suggest that an actin–myosin-based traction force plays only a minor role, if any, in the inward extension of furrow membrane during cellularization.

In the case of metaphase furrows, no defect in the behavior of other cytoskeleton components of the furrow (actin, anillin) is detectable in either sqh[1] embryos, after anti-MHC injection or after Rho kinase inhibition. Myosin II normally disappears from the furrow just as it is reaching its maximal depth (Foe *et al.,* 2000; Royou *et al.,* 2002) as part of the cycle of cortical recruitment and dispersion to which myosin II is subjected by the mitotic cycle. Thus, myosin II was unlikely to be required for its maintenance. Our results however exclude any critical role in initiating or positioning the metaphase furrow.

The major defects observed when myosin II is perturbed are seen during the fast phase of cellularization and in particular during the basal closure of the membrane rings in the final 20 min of cellularization. This process, requiring both actin and myosin II, but not microtubules, is also the part of cellularization most closely resembling true cytokinesis. We shall discuss the implications of this observation below.

What Is the Exact Nature of the Myosin II–containing Particles Found during Cellularization?

During the slow phase of cellularization, the furrow front is actively recruiting more myosin II from cytoplasmic stores (Figures 1 and 2). We have identified a population of myosin II-containing particles, ~1-μm diameter, that migrate to and fuse with the furrow front, apparently contributing to the local increase in myosin concentration. The myosin particles move apically by a mechanism requiring MTs. suggesting the involvement of a minus-end MT-based motor protein such as cytoplasmic dynein, which is involved in the transport of several kinds of cargo, including vesicles and mRNA (Vallee and Gee, 1998; Hays and Karess, 2000). Some two thirds of the GFP-myosin particles in fixed embryos are also associated with actin puncta (unpublished observations). Thus MT-based apical movement may provide a mechanism for recruiting to the furrow front several cortical components required for cellularization. By their behavior and intracellular location, they are also clearly distinguishable from the myosin VI–containing particles in the early embryo (Mermall *et al.,* 1994), which move on actin filaments.

Given the fact that we have been unable to find myosin II-containing particles of a similar size in fixed and immunostained wild-type embryos, it is certainly possible that they represent some kind of artifact related to the GFP tag on the RLC. However the RLC-GFP particles are themselves very sensitive to fixation conditions, requiring a special protocol (Rothwell and Sullivan, 2000) to be reliably preserved. One possibility therefore is that the RLC-GFP particles resist fixation slightly better than do the native myosin particles. A second possibility is that the large size of the RLC-GFP particle is artifactual, a consequence of aggregation via the GFP tag, but that the particles correspond nonetheless to the much smaller particles seen in wild-type embryos. (We note however that no such particles have ever been seen when other GFP tagged proteins are expressed in early embryos). In other words, if these particles are artifacts of the GFP fusion, they might simply be artifactually large aggregates, or artifactually stable to fixation. Nevertheless, their apically directed movement, their dependence on microtubules, their presence exclusively just before and during the slow phase of cellularization, and their ability to fuse seamlessly with the furrow front, all persuade us that they do represent a naturally occurring cytoplasmic source of myosin II.

Two Distinct Phases of Cellularization

That MTs and microfilaments are required for cellularization is well established (Zalokar and Erk, 1976; Foe and Alberts, 1983; Edgar *et al.,* 1987; Warn *et al.,* 1987; Sisson *et al.,* 2000). Treatment with colchicine or cytochalasin at the onset of cellularization completely inhibits furrow ingression just as it inhibits metaphase furrow invagination. Our in vivo studies have allowed us to refine the roles of these two cytoskeletal systems. The distinct phenotypes produced by perturbing MT function and actomyosin only after the onset of furrowing suggest that cellularization is composed to two partially independent processes: furrow ingression and basal closure.

We find that if cytochalasin is injected 20 min after cellularization has begun, the furrow continues to deepen significantly (see Figure 3). At the same time, this treatment severely disrupts the myosin network associated with the furrow front. Similarly, furrow formation and ingression is near normal when myosin II activity has been severely perturbed, as in sqh[1] embryos or after Y27632 treatment. Taken together, these results suggest that furrow invagination can occur with substantially reduced traction forces supplied by actin and myosin II. Instead, it may primarily rely on the lateral addition of Golgi-derived membrane vesicles as recently described (Burgess *et al.,* 1997; Lecuit and Wieschaus, 2000; Sisson *et al.,* 2000). Actin, however, is clearly still required for some aspects of furrowing, because early cytochalasin treatment entirely blocks furrowing onset, and the later treatment reduces both the rate of invagination and its final depth (unpublished data). In contrast to furrowing, there is an absolute requirement for both F-actin and myosin II during basal closure of the cells at the later phase of cellularization; perturbing either one leads to severe disruption of basal closure.

In embryos treated with colchicine 20 min after the onset of cellularization, furrow ingression nearly stopped, but myosin II remained at the furrow front, and in fact subsequently reorganized into contractile rings and progressively closed off the cells basally. Thus the role of MTs in furrow invagination might be primarily in transporting cytoplasmic membrane vesicles trafficking toward the furrow. Moreover, the fact that the myosin rings in these treated embryos contracted at the right time (~40 min into cellularization, corresponding to the period of the fast phase), suggests that cellularization can be divided into two distinct and semi-independent processes: 1) an inward-directed furrow extension perpendicular to the surface, dependent on MTs, and 2) a basal closure via cortical ring contraction parallel to the surface, requiring actin and myosin II.

A Revised Model for Cellularization

The conventional mechanistic model for cellularization involves an actin–myosin II network that forms a continuous structure during the early phase of cellularization, encompassing the whole embryo cortex. Contraction of the entire cortical network is assumed to produce an inwardly directed force that pulls membrane furrows toward the interior of the embryo in a plane perpendicular to the surface. When the furrows reach the basal level of the nuclei, the actin-myosin network divides into individual contractile rings that progressively decrease in diameter in a plane parallel to the surface of the embryo, thereby creating a conventional cleavage furrow and leading to basal closure.

Our experiments and other recent reports have led us to reassess the role of actin and myosin II in cellularization. We propose that although furrow establishment at the onset of cellularization depends on an intact actin network, its subsequent inward perpendicular invagination during the slow phase relies primarily on MT-dependent apico-lateral cytoplasmic vesicle fusion and requires relatively little traction force provided by actin and myosin II. The fast phase of furrow invagination is also at least partially independent of the actin–myosin network, as it too occurs, though less efficiently, in its

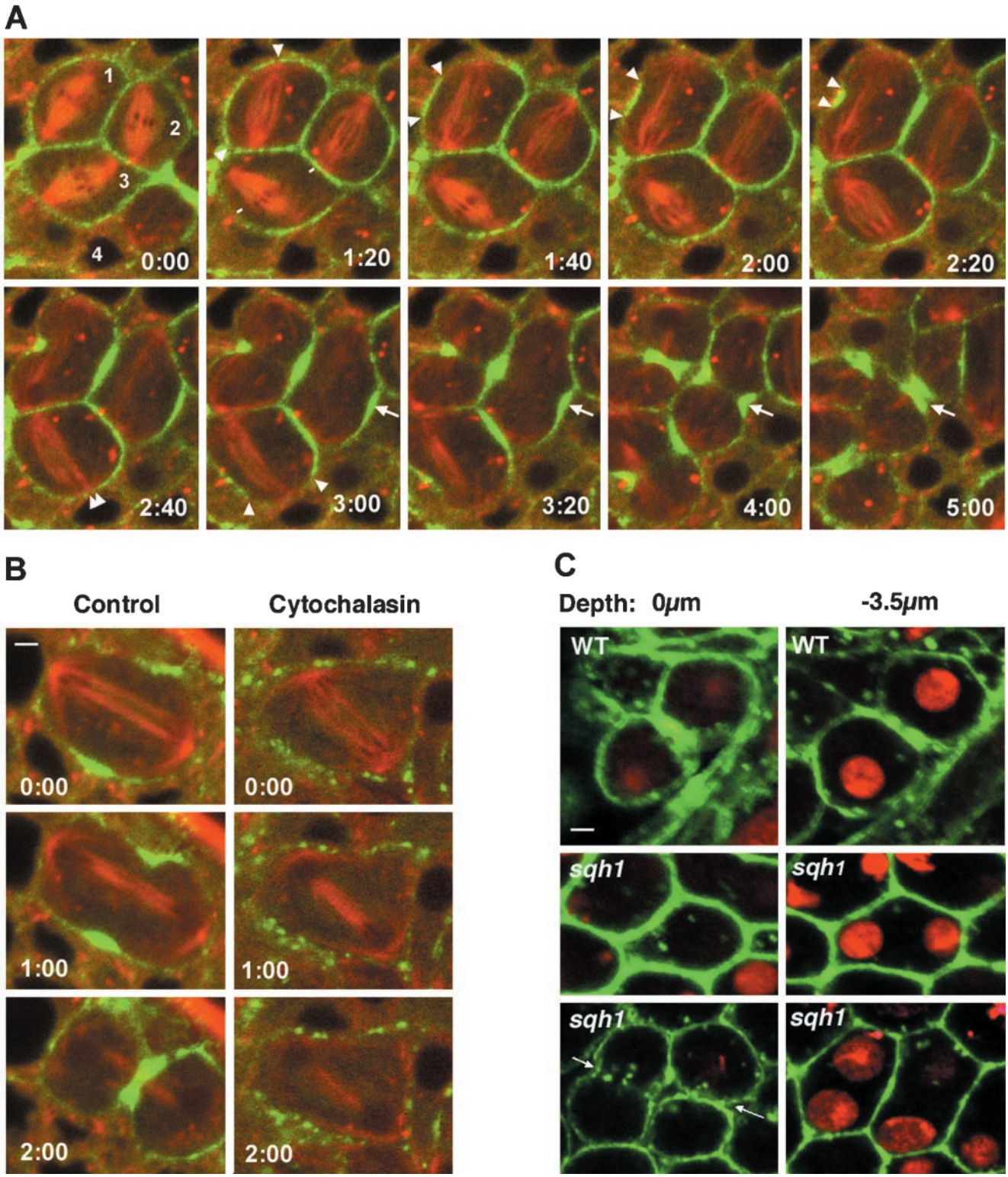

Figure 8. Myosin II dynamics visualized with RLC-GFP during the first divisions of the cellular blastoderm embryo. Syncytial stage RLC-GFP embryos were previously injected at their anterior poles with rhodamine-tubulin, to label spindles of the future cells. The first mitotic divisions after cellularization were recorded every 5 s. (A) A high magnification of a mitotic zone in the head. At interphase (e.g., cell 4), RLC-GFP fluorescence (green) is diffuse in the cytoplasm. During mitosis (cells 1, 2, 3) myosin II accumulates at the cortex as the cells round up. The spindle (labeled with rhodamine-tubulin, red) oscillates (compare cell 3 in the first two panels; stars). At anaphase, spindle movement stops and the RLC-GFP signal progressively declines from the poles and increases at the equator, suggesting cortical flow (follow arrowhead in cell 2 of the frames 1:20–2:40, and in cell 3 of frames 2:40–3:20). The newly formed myosin ring contracts, pinching off the cell in 2 min (arrow). See also Movie 5. (B) F-actin disruption prevents myosin ring formation and cytokinesis. RLC-GFP embryos injected with rhodamine-tubulin (red) and then injected with DMSO (control) or cytochalasin (0.1 mM) at the end of cellularization were monitored by

absence. By contrast, the final basal closure of the columnar cells does depend on actin–myosin-based contraction of the ring. In this model, only basal closure resembles conventional cytokinesis, in that both require the same contractile ring components such as actin, myosin II (Young *et al.,* 1991; Field and Alberts, 1995; Foe *et al.,* 2000), anillin (Field and Alberts, 1995; Miller and Kiehart, 1995), and septins (Neufeld and Rubin, 1994; Fares *et al.,* 1995; Adam *et al.,* 2000). The observation that the *Drosophila* septin Peanut, another cortical component that colocalizes with the actin–myosin network, is only required for basal closure during the later phase of cellularization is consistent with this model (Neufeld and Rubin, 1994; Fares *et al.,* 1995; Adam *et al.,* 2000).

The timing of basal closure is set relative to the onset of cellularization, not by the depth reached by the furrow. This conclusion is based on our observation that basal closure occurred even in colchicine-treated embryos, where the furrows had not passed beyond the level of the nuclei. That an independent mechanism regulates basal closure has also been suggested by the phenotype of the mutant *bottleneck* (Merrill *et al.,* 1988; Wieschaus and Sweeton, 1988; Schejter and Wieschaus, 1993). *bnk* mutant embryos show a premature rearrangement of the actin network during the slow phase of cellularization. Although the furrow begins to extend inward around the nuclei, the actin network forms distinct contractile units that prematurely close, often pinching off the apical portion of the nuclei, giving them a characteristic bottleneck appearance (Schejter and Wieschaus, 1993). At the onset of cellularization, Bnk protein colocalizes with cortical components at the furrow front and subsequently disappears from the front midway through cellularization. Its disappearance corresponds to the period when the actin–myosin network is rearranging into separated rings that will later carry out basal closure. Thus Bnk might be preventing premature constriction of the cortical actin–myosin rings by tightly and physically linking these cortical components during the earlier phase of cellularization. Analysis of myosin II dynamics during cellularization in live *bnk* mutant embryos using the GFP-RLC marker should also provide critical information about this process.

Myosin II and Cytokinesis

Although observing myosin II dynamics during conventional cytokinesis in the first divisions of early gastrulation, we found that myosin II is recruited uniformly to the cortex as the cell rounds up upon entering mitosis. At late anaphase, cortical myosin II begins sliding along the cortex from the polar to equatorial regions to form the contractile ring at the future cleavage site. This strongly suggests that cortical flow is responsible for concentrating myosin II at the cleavage plane, as has been documented recently during cytokinesis in *Dictyostelium* (Yumura, 2001). At the end of this reorganization, the myosin ring contracts, providing the force that pulls the cleavage furrow inward. Cortical myosin recruitment at the onset of mitosis occurs even in the absence of actin after cytochalasin treatment, athough the myosin is no longer evenly distributed around the cortex. Presumably as a consequence the cell does not round up. Thus myosin II recruitment to the cortex at the onset of mitosis may provide some of the cortical tension that helps the cell to change from a columnar to a spherical shape appropriate for mitosis and cytokinesis.

Figure 8 (facing page). TLCM during the first head divisions at gastrulation stage. In the control embryo, myosin II accumulates at the equator of the cell to form a ring that contracts at telophase. After disruption of the actin network, myosin still accumulates at the cortex but only in irregular lumps. At telophase, myosin fails to reorganize into a ring at the equator of the cell, and no cleavage furrow forms. (Scale bar, 2 μm). (C) Cytokinesis is disrupted in sqh^1 embryos. Wild-type embryo (top) and two different sqh^1 embryos (bottom 2 panels) were fixed and stained with phalloidin (green) and propidium iodide (red) and analyzed by confocal microscopy. In WT embryos, the actin-rich cleavage furrow is clearly dividing the cell in two (at telophase). No cleavage furrows are formed in telophase cells of sqh^1 embryo (second row). Sometimes cleavage furrows form at the apical side of the cells (arrows, third row) but disappear deeply in the cell (-3.5 μm). In addition, the mutant cells in sqh^1 embryos appear not to round up fully. (Scale bar, 2 μm).

RLC-GFP Is a Good Marker for Studying Myosin II–based Processes

The transgene expressing the C-terminal fusion of GFP to RLC produces a fully functional protein, capable of rescuing the *sqh^{AX3}* null mutation to fertile adulthood, with no apparent abnormal phenotype. The protein colocalizes both spatially and temporally with MHC wherever it has been examined. It thus provides an excellent tool for studying myosin II dynamics in vivo. The ability to monitor myosin II in vivo should lead to a better understanding of its role in carrying out the cell shape changes essential for cell division and morphogenesis during *Drosophila* development.

ACKNOWLEDGMENTS

We thank Tom Hays for insights, musings, and helpful discussions; Spencer Brown and Michel Laurent for help with confocal microscopy; and Jeremy Thiblet for his helpful advice in using the Metaview imaging system. This work was supported in part by grants to R.K. from the French CNRS and the Association Pour la Recherche sur le Cancer (ARC), to W.S from National Institutes of Health Grant GM46409 and the France/Berkeley fund. A.R. was supported by Le Ministèredel'Education Nationale dela recherche et dela technologie and ARC (Paris, France). The Gif confocal facility was supported by IFR87 "La plante et son environment" and the Conseil Général del'Essonne (Programme ASTRE).

REFERENCES

Adam, J.C., Pringle, J.R., and Peifer, M. (2000). Evidence for functional differentiation among Drosophila septins in cytokinesis and cellularization. Mol. Biol. Cell *11,* 3123–3135.

Afshar, K., Stuart, B., and Wasserman, S.A. (2000). Functional analysis of the Drosophila Diaphanous FH protein in early embryonic development. Development *127,* 1887–1897.

Amano, M., Ito, M., Kimura, K., Fukata, Y., Chihara, K., Nakano, T., Matsuura, Y., and Kaibuchi, K. (1996). Phosphorylation and activation of myosin by Rho-associated kinase (Rho-kinase). J. Biol. Chem. *271,* 20246–20249.

Burgess, R.W., Deitcher, D.L., and Schwarz, T.L. (1997). The synaptic protein syntaxin1 is required for cellularization of Drosophila embryos. J. Cell Biol. *138,* 861–875.

Chou, T.B., Noll, E., and Perrimon, N. (1993). Autosomal P[ovoD1] dominant female-sterile insertions in Drosophila and their use in generating germ-line chimeras. Development *119,* 1359–1369.

Chou, T.B., and Perrimon, N. (1992). Use of a yeast site-specific recombinase to produce female germline chimeras in Drosophila. Genetics *131,* 643–653.

Edgar, B.A., Odell, G.M., and Schubiger, G. (1987). Cytoarchitecture and the patterning of fushi tarazu expression in the Drosophila blastoderm. Genes Dev. *1,* 1226–1237.

Edwards, K.A., Demsky, M., Montague, R.A., Weymouth, N., and Kiehart, D.P. (1997). GFP-moesin illuminates actin cytoskeleton dynamics in living tissue and demonstrates cell shape changes during morphogenesis in Drosophila. Dev. Biol. *191,* 103–117.

Edwards, K.A., and Kiehart, D.P. (1996). Drosophila nonmuscle myosin II has multiple essential roles in imaginal disc and egg chamber morphogenesis. Development *122,* 1499–1511.

Fares, H., Peifer, M., and Pringle, J.R. (1995). Localization and possible functions of Drosophila septins. Mol. Biol. Cell *6,* 1843–1859.

Field, C.M., al-Awar, O., Rosenblatt, J., Wong, M.L., Alberts, B., and Mitchison, T.J. (1996). A purified Drosophila septin complex forms filaments and exhibits GTPase activity. J. Cell Biol. *133,* 605–616.

Field, C.M., and Alberts, B.M. (1995). Anillin, a contractile ring protein that cycles from the nucleus to the cell cortex. J. Cell Biol. *131,* 165–178.

Foe, V., and Alberts, B. (1983). Studies of nuclear and cytoplasmic behavior during the five mitotic cycles that precede gastrulation in Drosophila embryogenesis. J. Cell Sci. *61,* 31–70.

Foe, V., Odell, G., and Edgar, B. (1993). Mitosis and morphogenesis in the Drosophila embryo: point and counterpoint. In: The Development of *Drosophila melanogaster,* Vol. 1, ed. A. Martinez-Arias, Cold Spring Harbor, NY: Cold Spring Harbor Laboratory Press, 149–300.

Foe, V.E., Field, C.M., and Odell, G.M. (2000). Microtubules and mitotic cycle phase modulate spatiotemporal distributions of F-actin and myosin II in Drosophila syncytial blastoderm embryos. Development *127,* 1767–1787.

Francis-Lang, H., Minden, J., Sullivan, W., and Oegema, K. (1999). Live confocal analysis with fluorescently labeled proteins. Methods Mol. Biol. *122,* 223–239.

Fukata, Y., Amano, M., and Kaibuchi, K. (2001). Rho-Rho-kinase pathway in smooth muscle contraction and cytoskeletal reorganization of non-muscle cells. Trends Pharmacol. Sci. *22,* 32–39.

Giansanti, M.G., Bonaccorsi, S., Williams, B., Williams, E.V., Santolamazza, C., Goldberg, M.L., and Gatti, M. (1998). Cooperative interactions between the central spindle and the contractile ring during Drosophila cytokinesis. Genes Dev. *12,* 396–410.

Glotzer, M. Animal cell cytokinesis. Ann, Rev. Cell Dev. Biol. *17,* 351–386.

Hays, T., and Karess, R. (2000). Swallowing dynein: a missing link in RNA localization? Nat. Cell Biol. *2,* E60–E62.

Jordan, P., and Karess, R. (1997). Myosin light chain-activating phosphorylation sites are required for oogenesis in Drosophila. J. Cell Biol. *139,* 1805–1819.

Karess, R.E., Chang, X., Edwards, K.A., Kulkarni, S., Aguilera, I., and Kiehart, D.P. (1991). The regulatory light chain of nonmuscle myosin is encoded by spaghetti-squash, a gene required for cytokinesis in drosophila. Cell *65,* 1177–1189.

Karr, T., and Alberts, B. (1986). Organization of the cytoskeleton in early Drosophila embryos. J. Cell Biol. *98,* 156–162.

Kiehart, D.P. (1990). Molecular genetic dissection of myosin heavy chain function. Cell *60,* 347–350.

Kiehart, D.P. *et al.* (1990). Contractile proteins in Drosophila development. Ann. NY Acad. Sci. *582,* 233–251.

Kimura, K. *et al.* (1996). Regulation of myosin phosphatase by Rho and Rho-associated kinase (Rho-kinase). Science *273,* 245–248.

Lecuit, T., and Wieschaus, E. (2000). Polarized insertion of new membrane from a cytoplasmic reservoir during cleavage of the Drosophila embryo. J. Cell Biol. *150,* 849–860.

Mermall, V., McNally, J.G., and Miller, K.G. (1994). Transport of cytoplasmic particles catalysed by an unconventional myosin in living Drosophila embryos. Nature *369,* 560–562.

Mermall, V., and Miller, K.G. (1995). The 95F unconventional myosin is required for proper organization of the Drosophila syncytial blastoderm. J. Cell Biol. *129,* 1575–1588.

Merrill, P.T., Sweeton, D., and Wieschaus, E. (1988). Requirements for autosomal gene activity during precellular stages of Drosophila melanogaster. Development *104,* 495–509.

Miller, K.G., Field, C.M., and Alberts, B.M. (1989). Actin-binding proteins from Drosophila embryos: a complex network of interacting proteins detected by F-actin affinity chromatography. J. Cell Biol. *109,* 2963–2975.

Miller, K.G., and Kiehart, D.P. (1995). Fly division. J. Cell Biol. *131,* 1–5.

Narumiya, S., Ishizaki, T., and Uehata, M. (2000). Use and properties of ROCK-specific inhibitor Y-27632. Methods Enzymol. *325,* 273–284.

Neufeld, T.P., and Rubin, G.M. (1994). The Drosophila peanut gene is required for cytokinesis and encodes a protein similar to yeast putative bud neck filament proteins. Cell *77,* 371–379.

Pirrotta, V. (1988). Vectors for P-mediated transformation in Drosophila. Biotechnology *10,* 437–456.

Ripoche, J., Link, B., Yucel, J.K., Tokuyasu, K., and Malhotra, V. (1994). Location of Golgi membranes with reference to dividing nuclei in syncytial Drosophila embryos. Proc. Natl. Acad. Sci. USA *91,* 1878–1882.

Rothwell, W.F., and Sullivan, W. (2000). Fluorescent Analysis of Drosophila embryos. In: Drosophila protocols, ed. R. S. Hawley, Cold Spring Harbor, NY: Cold Spring Harbor Laboratory Press, 141–157.

Rothwell, W.F., Zhang, C.X., Zelano, C., Hsieh, T.s., and Sullivan, W. (1999). The Drosophila centrosomal protein nuf is required for recruiting dah, a membrane associated protein, to furrows in the early embryo [In Process Citation]. J. Cell Sci. 2885–2893.

Royou, A., Sullivan, W., and Karess, R. (2002). Cortical recruitment of nonmuscle myosin II in early syncytial Drosophila embryos: its role in nuclear axial expansion and its regulation by Cdc2 activity. J. Cell Biol. *158,* 127–137.

Schejter, E.D., Rose, L.S., Postner, M.A., and Wieschaus, E. (1992). Role of the zygotic genome in the restructuring of the actin cytoskeleton at the cycle-14 transition during Drosophila embryogenesis. Cold Spring Harb. Symp. Quant. Biol. *57,* 653–659.

Schejter, E.D., and Wieschaus, E. (1993). Functional elements of the cytoskeleton in the early Drosophila embryo. Annu. Rev. Cell Biol. *9,* 67–99.

Schweisguth, F., Lepesant, J.A., and Vincent, A. (1990). The serendipity alpha gene encodes a membrane-associated protein required for the cellularization of the Drosophila embryo. Genes Dev. *4,* 922–931.

Simpson, L., and Wieschaus, E. (1990). Zygotic activity of the nullo locus is required to stabilize the actin-myosin network during cellularization in Drosophila. Development *110,* 851–863.

Sisson, J.C., Field, C., Ventura, R., Royou, A., and Sullivan, W. (2000). Lava lamp, a novel peripheral golgi protein, is required for Drosophila melanogaster cellularization. J. Cell Biol. *151,* 905–918.

Stafstrom, J.P., and Staehelin, L.A. (1984). Dynamics of the nuclear envelope and of nuclear pore complexes during mitosis in the Drosophila embryo. Eur J. Cell Biol. *34,* 179–189.

Straight, A.F., and Field, C.M. (2000). Microtubules, membranes and cytokinesis. Curr. Biol. *10,* R760–R770.

Sullivan, W., Minden, J.S., and Alberts, B.M. (1990). daughterless-abo-like, a Drosophila maternal-effect mutation that exhibits abnormal centrosome separation during the late blastoderm divisions. Development *110,* 311–323.

Sullivan, W., and Theurkauf, W.E. (1995). The cytoskeleton and morphogenesis of the early Drosophila embryo. Curr. Opin. Cell Biol. *7,* 18–22.

Vallee, R.B., and Gee, M.A. (1998). Make room for dynein. Trends Cell Biol. *8,* 490–494.

Warn, R.M., Bullard, B., and Magrath, R. (1980). Changes in the distribution of cortical myosin during the cellularization of the Drosophila embryo. J. Embryol. Exp. Morphol. *57,* 167–176.

Warn, R.M., Flegg, L., and Warn, A. (1987). An investigation of microtubule organization and functions in living Drosophila embryos by injection of a fluorescently labeled antibody against tyrosinated alpha-tubulin. J. Cell Biol. *105,* 1721–1730.

Warn, R.M., and Magrath, R. (1983). F-actin distribution during the cellularization of the Drosophila embryo visualized with FL-phalloidin. Exp. Cell Res. *143,* 103–114.

Warn, R.N., and Robert-Nicoud, M. (1990). F-actin organization during the cellularization of the Drosophila embryo as revealed with a confocal laser scanning microscope. J. Cell Sci. *96,* 35–42.

Wheatley, S., Kulkarni, S., and Karess, R. (1995). Drosophila nonmuscle myosin II is required for rapid cytoplasmic transport during oogenesis and for axial nuclear migration in early embryos. Development *121,* 1937–1946.

Wieschaus, E., and Sweeton, D. (1988). Requirements for X-linked zygotic gene activity during cellularization of early Drosophila embryos. Development *104,* 483–493.

Winter, C.G., Wang, B., Ballew, A., Royou, A., Karess, R., Axelrod, J.D., and Luo, L. (2001). Drosophila Rho-associated kinase (Drok) links Frizzled-mediated planar cell polarity signaling to the actin cytoskeleton. Cell *105,* 81–91.

Young, P.E., Pesacreta, T.C., and Kiehart, D.P. (1991). Dynamic changes in the distribution of cytoplasmic myosin during Drosophila embryogenesis. Development *111,* 1–14.

Yumura, S. (2001). Myosin II dynamics and cortical flow during contractile ring formation in Dictyostelium cells. J. Cell Biol. *154,* 137–146.

Zalokar, M., and Erk, I. (1976). Division and migration of nuclei during early embryogenesis of Drosophila melanogaster. J. Microsc. Biol. Cell *25,* 97–106.

Zhang, C.X., Rothwell, W.F., Sullivan, W., and Hsieh, T.S. (2000). Discontinuous actin hexagon, a protein essential for cortical furrow formation in Drosophila, is membrane associated and hyperphosphorylated. Mol. Biol. Cell *11,* 1011–1022.